IEEE Access
Multidisciplinary | Rapid Review | Open Access Journal

Received May 13, 2019, accepted July 19, 2019, date of publication July 30, 2019, date of current version September 25, 2019.

Digital Object Identifier 10.1109/ACCESS.2019.2932092

Sliding-Mode Flux-Weakening Control With Only Single Current Regulator for Permanent Magnet Synchronous Motor

XUE LI[1,2], CONG LIU[1,2], SHANG WU[1,2], SONG CHI[1,2], (Member, IEEE), AND POH CHIANG LOH[3]

[1]State Key Laboratory of Reliability and Intelligence of Electrical Equipment, Hebei University of Technology, Tianjin 300130, China
[2]Hebei Key Laboratory of Electromagnetic Field and Electrical Apparatus Reliability, Hebei University of Technology, Tianjin 300130, China
[3]Department of Electronic Engineering, The Chinese University of Hong Kong, Hong Kong

Corresponding author: Song Chi (chis@hebut.edu.cn)

This work supported by the Research on High Frequency Power Electronic Technology and Application (“100 People Plan” Funding for Introducing Overseas High-level Talents of Hebei Province) under Grant E2015100007.

ABSTRACT A sliding-mode scheme using only a single current regulator for both speed and flux-weakening control has been proposed for permanent magnet synchronous motor. The scheme is simple and can effectively resolve problems faced by conventional flux-weakening control with dual current regulation loops. However, with only a single current regulator, the scheme still needs an additional mechanism for either maximizing electromagnetic torque or optimizing efficiency. As for reinforcing its immunity and robustness towards changing operating conditions, sliding-mode speed control complemented by an equivalent load-torque observer during flux-weakening has been proposed and designed accordingly. Effectiveness of the eventual scheme, in terms of widening load capacity or improving light-load efficiency of the motor, has been verified in simulations and experiments.

INDEX TERMS Permanent magnet synchronous motor, flux-weakening control, sliding-mode control, single current regulator.

I. INTRODUCTION

With the invention of permanent magnet materials, permanent magnet synchronous machines (PMSMs) have been increasingly used as industrial drives for rail transit, wind power generation, and aerospace to name only a few. Each of these PMSM drives, in turn, requires a large starting torque and must operate over a wide speed range with high efficiency and power density. In other words, it must operate in both constant-torque region when its speed is low and constant-power region when its speed is high. Where necessary, its speed range can further be widened by weakening its flux. This has traditionally been implemented with field-oriented control (FOC), where there are two control loops for regulating the d- and q-axis currents, respectively notated as i_d and i_q.

Because of that, it is common to plan the PMSM stator current trajectory on the $i_d - i_q$ coordinate plane during flux-weakening. One such plan depends on extensive calculation with formulas, which in [1] and [2], has been referred to as the formula-calculation method. This method depends heavily on motor parameters, which in practice, will usually vary. Alternatively, the flux-weakening trajectory can be realized with a look-up table, but only if lots of experimental data are available or portability is not an issue [3]–[5] Otherwise, the gradient-descent method can be considered for finding the flux-weakening region, according to tangential direction of the torque curve and angle of the voltage-limit ellipse. That method is however burdened by overly complicated computation [6].

Other methods therefore opt to regulate the PMSM current directly during flux-weakening. One example is the commonly used method from [7] and [8], where the negative d-axis current has been compensated by a voltage regulator. Another two examples can be found in [9] and [10], where either the current command has been tuned according to the current error or the d-axis current i_d has been adjusted according to the duty cycle. These are undoubtedly new ideas

The associate editor coordinating the review of this manuscript and approving it for publication was Jun Hu.

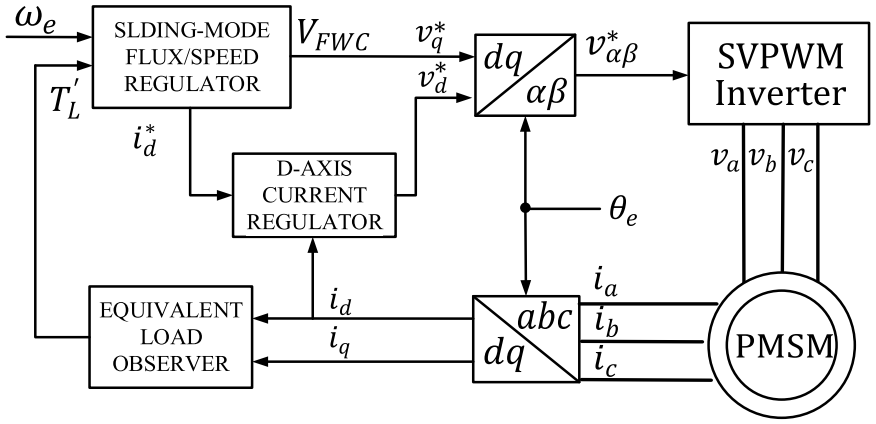

FIGURE 1. Overall block diagram of proposed flux-weakening scheme.

and analytical techniques for PMSM flux-weakening control, but have traditionally been implemented with two current regulators for torque and flux control. The shortcoming here is non-negligible cross-coupling between both regulators during flux-weakening, which strengthens with an increase in speed. Both regulators therefore saturate easily, causing the motor performance to degrade.

This leads [11] to propose a novel flux-weakening scheme for PMSM, which relies only on a single current regulator, so as to avoid the aforementioned saturation. That scheme also does not require knowledge of the motor parameters and dc-bus voltage of the inverter. It nevertheless does not allow the motor to fully utilize dc-bus voltage of its driving inverter. Its unintended side-effects are thus a narrower speed range, smaller load capacity and poorer motor efficiency. These side-effects can be mitigated by finding the q-axis voltage through offline calculation and online checking of a lookup table, as explained in [12]–[14]. But, with its lookup table, the usual problems of requiring lots of experimental data and lacking portability have resurfaced.

Another issue with most existing PMSM drives is their reliance on only linear proportional-integral (PI) controllers, which unquestionably is convenient to set up and easy to understand. However, a PMSM is a complex nonlinear entity with varying parameters and multiple strongly coupled variables. It is therefore not possible for PI control to generate the desired responses over the full operating range, especially with changes of motor or other external parameters. In this paper, a sliding-mode scheme with only a single current regulator has hence been proposed for PMSM control during flux-weakening. The proposed scheme can achieve either electromagnetic-torque maximization or efficiency optimization over its full speed range. Moreover, with sliding-mode speed control during flux-weakening, immunity and robustness of the overall PMSM drive can be ensured. Simulation and experimental results have demonstrated these expectations by explicitly showing an improvement in load capacity or light-load efficiency.

II. FLUX-WEAKENING CONTROL WITH SINGLE CURRENT REGULATOR

A block diagram for showing the overall proposed scheme is given in Fig. 1, where as usual, the three-phase motor currents i_a, i_b and i_c have been measured and transformed to the d- and q-axis currents i_d and i_q. The transformed currents have then been traditionally regulated by two inner control loops to generate modulating voltages v_d^* and v_q^*. This changes with only a single current regulator, or more precisely, an alternative mechanism must now be formulated for finding one of the modulating voltages. With the proposed scheme, it is to find v_q^* during flux-weakening, while satisfying either electromagnetic-torque maximization or efficiency optimization for the PMSM. More details about both criterions related to finding v_q^* can be found in Section III, after explaining limitations obeyed by the single current regulator in this section.

A. CURRENT AND VOLTAGE LIMITS

The general expression for modeling a PMSM with ($L_d \neq L_q$) in the rotor reference frame is given below:

$$\begin{bmatrix} v_d \\ v_q \end{bmatrix} = \begin{bmatrix} R_s + pL_d & -\omega_e L_q \\ \omega_e L_d & R_s + pL_q \end{bmatrix} \begin{bmatrix} i_d \\ i_q \end{bmatrix} + \begin{bmatrix} 0 \\ \omega_e \psi_f \end{bmatrix} \quad (1)$$

where v, i, L and R_s are voltage, current, inductance and resistance of the stator, subscripts d and q are for notating d- and q-axes, ω_e is the electrical angular velocity of the rotor, ψ_f is the permanent magnetic flux, and $p = d/dt$ is the derivative operator. In the steady state, all derivatives are zero. Equation (1) then becomes:

$$\begin{bmatrix} V_d \\ V_q \end{bmatrix} = \begin{bmatrix} R_s & -\omega_e L_q \\ \omega_e L_d & R_s \end{bmatrix} \begin{bmatrix} I_d \\ I_q \end{bmatrix} + \begin{bmatrix} 0 \\ \omega_e \psi_f \end{bmatrix} \quad (2)$$

where V and I are steady-state values of variables v and i, respectively.

On the other hand, electromagnetic torque developed by the motor can be expressed as:

$$T_e = \frac{3}{2} n_p \left[\psi_f I_q + \left(L_d - L_q \right) I_d I_q \right] \quad (3)$$

where n_p is the number of pole pairs. Additionally, the maximum stator voltage V_{smax} of the PMSM depends on dc-bus voltage V_{dc} and modulation scheme of the inverter.

In case of space-vector pulse-width modulation (SVPWM), V_{smax} becomes $V_{dc}/\sqrt{3}$, which indirectly means V_d and V_q must satisfy:

$$V_d^2 + V_q^2 \leq \left(V_{smax}^2 = V_{dc}^2 \Big/ 3\right) \tag{4}$$

Substituting (2) to (4) then leads to:

$$\left(\frac{R_s I_d}{\omega_e} - L_q I_q\right)^2 + \left(\frac{R_s I_q}{\omega_e} + L_d I_d + \psi_f\right)^2 \leq \left(\frac{V_{smax}}{\omega_e}\right)^2 \tag{5}$$

if with stator resistance R_s neglected, simplifies to:

$$\left(L_q I_q\right)^2 + \left(L_d I_d + \psi_f\right)^2 \leq \left(\frac{V_{smax}}{\omega_e}\right)^2 \tag{6}$$

Inequality (6) is obviously an ellipse on the $i_d - i_q$ plane, whose size depends on V_{smax} (and ω_e). It is thus referred to as the voltage-limit boundary, within which all operating point $\left(I_d, I_q\right)$ must remain at a particular frequency. Besides (6), the operating point must satisfy:

$$I_d^2 + I_q^2 \leq I_{smax}^2 \tag{7}$$

where I_{smax} is the maximum stator current limited by capacity of the inverter and temperature rise of the PMSM. However, unlike (6), (7) is a circle in the $i_d - i_q$ plane, whose size depends only on I_{smax}. Inequality (7) is thus a current-limit boundary, within which all operating point $\left(I_d, I_q\right)$ must remain.

B. TRAJECTORY OF SINGLE CURRENT REGULATOR WITHIN LIMITS

Between the d- and q-axis currents, coupling exists and can be derived from (2) as:

$$I_q = -\frac{\omega_e L_d}{R_s} I_d + \frac{V_q - \psi_f \omega_e}{R_s} \tag{8}$$

$$I_q = K_i\left(\omega_e\right) I_d + B_i(\omega_e, V_q) \tag{9}$$

where

$$K_i\left(\omega_e\right) = -\frac{\omega_e L_d}{R_s} = gradient$$

$$B_i\left(\omega_e, V_q\right) = \frac{V_q - \psi_f \omega_e}{R_s} = q - axis\ intercept$$

They remain unchanged during flux-weakening, except with V_q replaced by the reduced flux-weakening-control voltage V_{FWC}. After the replacement, the expressions become:

$$I_q = -\frac{\omega_e L_d}{R_s} I_d + \frac{V_{FWC} - \psi_f \omega_e}{R_s} \tag{10}$$

$$I_q = K_i I_d + B_i \tag{11}$$

where

$$K_i = -\frac{\omega_e L_d}{R_s} = gradient$$

$$B_i = \frac{V_{FWC} - \psi_f \omega_e}{R_s} = q - axis\ intercept$$

Therefore, with a known set of speed $\omega_e(\neq 0)$ and voltage V_{FWC}, only a single current regulator is essential for determining either I_d or I_q independently. The other current can then be linearly calculated from (11), if necessary. The same applies to demagnetizing effect and electromagnetic torque in (3), since (11) infers that they can be controlled by either I_d or I_q only, if ω_e and V_{FWC} are known. Graphically, the linear (11) with ω_e and V_{FWC} given can be drawn together with the elliptical voltage-limit boundary from (6) and circular current-limit boundary from (7).

Particularly, with ω_e fixed as a constant varying V_{FWC} causes the negative-sloping line to move with the same gradient K_i, but with different q-axis intercepts. On the other hand, with V_{FWC} fixed varying ω_e causes both gradient and q-axis intercept to change. Linear lines representing (11) are thus no longer parallel. Regardless of that, the conclusion drawn is the linear operating range of a PMSM can be controlled, and in most cases, it is through adjusting V_{FWC} along the q-axis, since ω_e is usually regulated by the outer speed controller. An appropriate mechanism for selecting V_{FWC} is thus vital for use with the single current regulator. Their eventual purpose is to generate modulating voltages v_d^* and $v_q^* = V_{FWC}$. More information about V_{FWC} is thus essential, as provided next.

III. FLUX-WEAKENING VOLTAGE DETERMINATION

A. LIMITED-VOLTAGE MAXIMUM-TORQUE CRITERION

At all times and frequencies, an operating point of the PMSM must satisfy the voltage-limit ellipse defined by (6) and current-limit circle defined by (7). Ideally, it should further be on either one or both boundaries to utilize the motor capacity fully for generating maximum torque. Torque T_e can, in turn, be derived from (3), (6) and (7) at maximum stator voltage V_{smax}. The obtained expression is given below:

$$T_e = \frac{3}{2} n_p \left[\frac{\psi_f}{L_q} k_2 + k_1 k_2 I_d\right] \tag{12}$$

where

$$k_1 = \frac{\left(L_d - L_q\right)}{L_q}$$

$$k_2 = \sqrt{\left(\frac{V_{smax}}{\omega_e}\right)^2 - \left(L_d I_d + \psi_f\right)^2}$$

Derivative of T_e with respect to I_d can then be derived as:

$$\frac{dT_e}{dI_d} = \frac{3n_p}{2}\left[k_1 k_2 + \left(\frac{\psi_f}{L_q} + k_1 I_d\right)\frac{dk_2}{dI_d}\right] \tag{13}$$

where

$$\frac{dk_2}{dI_d} = \frac{L_d\left(L_d I_d + \psi_f\right)}{k_2}$$

Equating (13) to zero eventually allows I_d at maximum torque to be determined as:

$$I_d = \frac{1}{L_d}\left[\frac{\psi_f}{4k_1} - \frac{1}{4}\sqrt{\left(\frac{\psi_f}{k_1}\right)^2 + 8\left(\frac{V_{smax}}{\omega_e}\right)^2} - \psi_f\right] \tag{14}$$

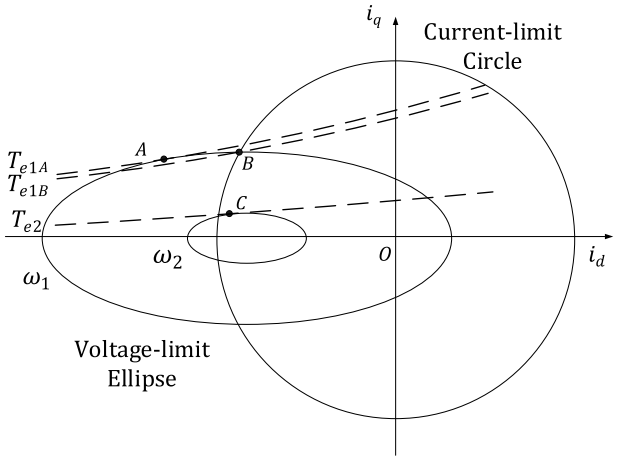

FIGURE 2. Illustration of limited-voltage maximum-torque criterion during flux-weakening.

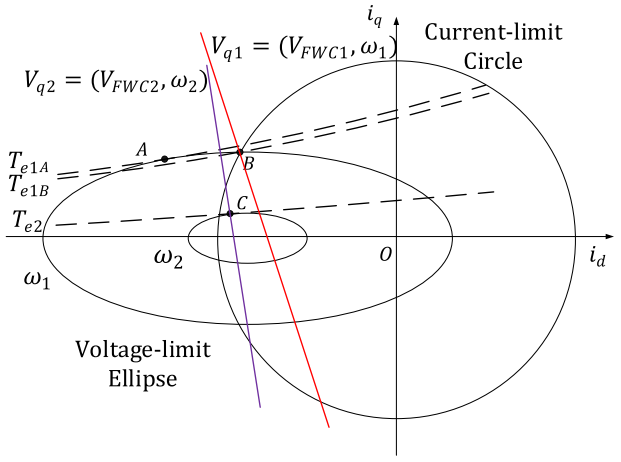

FIGURE 3. Tuning of flux-weakening voltages and linear current trajectories to satisfy limited-voltage maximum-torque criterion at different speeds.

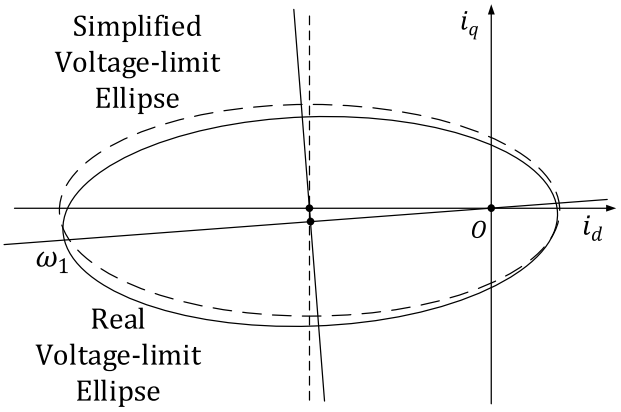

FIGURE 4. Tilting of voltage-limit ellipse caused by non-negligible stator resistance.

In the $i_d - i_q$ plane in Fig. 2, this maximum operating point with maximized load capacity corresponds to a single tangential point formed by two curves. The first can be the voltage-limit ellipse at $\omega_e = \omega_1$, while the second can be the constant-torque curve plotted with (3) and $T_e = T_{e1A}$. Their resulting tangential point has been marked as A in the second quadrant of Fig. 2. Point A is however outside the current-limit circle and hence not a permissible operating point for the PMSM. The next closest operating point B must hence be assumed, which in Fig. 2, is the intersection of the same voltage-limit ellipse, current-limit circle and a second constant-torque curve plotted with $T_e = T_{e1B}$.

Such adjustment is not necessary at higher speed $\omega_e = \omega_2$, whose accompanied voltage-limit ellipse is smaller, as seen from Fig. 2. The new maximum-torque tangential point is then at point C, formed by the smaller ellipse and third constant-torque curve drawn with $T_e = T_{e2}$. No adjustment is now needed, since point C, being inside the current-limit circle, is a permissible operating point. In conclusion, a set of unique maximum-torque points at all operating speeds can be computed for the PMSM to form its operating range with maximum permissible output torque always generated. Each maximum-torque point can then be tracked by the single current regulator and mechanism for tuning V_{FWC} along the q-axis are represented by negatively sloping linear current trajectories. The target is to control each line to pass through its corresponding maximum-torque point at the same considered speed ω_e.

This target, also named as limited-voltage maximum-torque criterion, is better illustrated with Fig. 3 during flux-weakening. For example, when $\omega_e = \omega_1$, the maximum-torque point is at B, which then requires the flux-weakening voltage to be set to V_{FWC1}, so that its associated linear current trajectory passes through point B at the same considered speed of ω_1. Subsequently, when ω_e increases to ω_2, the maximum-torque point shifts to C and the new flux-weakening voltage must be changed to V_{FWC2} to again direct the new linear current trajectory to pass through point C at the higher ω_2. It is thus possible to control the PMSM to always output maximum torque, while staying within voltage and current limits, by simply using only a single current regulator and a mechanism for finding the proper flux-weakening voltage.

The above analysis is however proceeded with stator resistance and its voltage drop neglected. Their effects, if included, are shown in Fig. 4, where it can be seen that they cause the voltage-limit ellipse to shift from its earlier dotted position to its new tilted position. The amount of tilting can be found from (5), which upon analyzed, permits symmetrical axes of the tilted ellipse to be expressed as:

$$\begin{cases} I_q = \dfrac{R_s}{L_q \omega_e} I_d & (horizontal) \\ I_d = \dfrac{R_s}{\omega_e L_d} I_q - \dfrac{\psi_f}{L_d} & (vertical) \end{cases} \tag{15}$$

The horizontal axis is thus tilted by $\tan^{-1}\left(R_s/\omega_e L_q\right)$ about the origin, while the vertical axis is tilted by $\tan^{-1}\left(R_s/\omega_e L_d\right)$ about the point $\left(0, -\psi_f/L_d\right)$, rather than the origin.

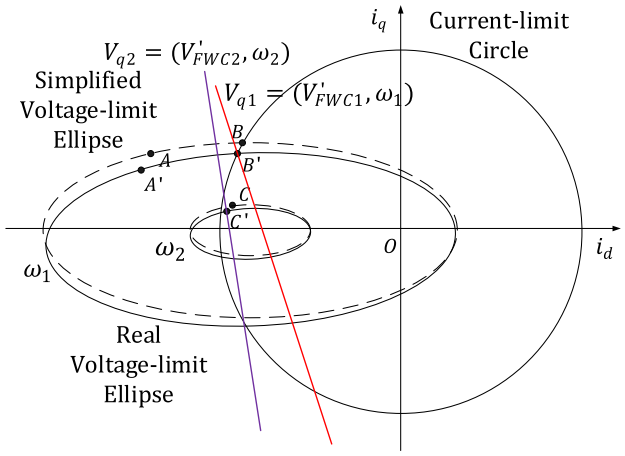

FIGURE 5. Shifting of maximum-torque operating points caused by non-negligible stator resistance.

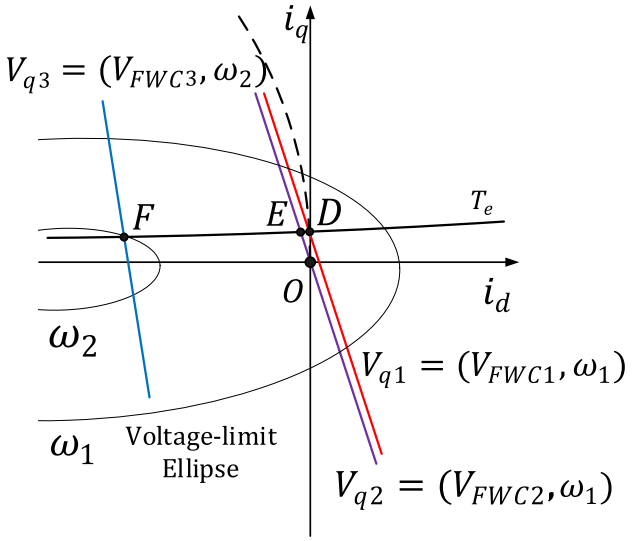

FIGURE 6. Tuning of flux-weakening voltages and linear current trajectories to satisfy optimized-efficiency criterion at different speeds.

Other than those, the size and shape of the ellipse remain unchanged, which in the second quadrant, causes operating range of the PMSM to drop slightly. This drop is better illustrated with Fig. 5, where the tilted voltage-limit ellipse has caused maximum-torque points to shift from B to B' and C to C'. These new points have smaller maximum torques at their respective speeds in the second quadrant, but irrespective of that, values for V_{FWC} must be lowered, so that their corresponding linear current trajectories continue to intersect with points B' and C'. The presence of state resistance has therefore not changed the underlying operating principles.

B. EFFICIENCY-OPTIMIZED CRITERION

To optimize efficiency, amplitude of the d-q current vector must be minimized. According to Lagrange Multiplier, the objective function can thus be expressed as:

$$f = I_s = \sqrt{I_d^2 + I_q^2} \tag{16}$$

with its constraint given in (3). A Lagrange function can then be constructed like shown below:

$$F = \sqrt{I_d^2 + I_q^2} + \lambda \left\{ T_e - \frac{3}{2} n_p \left[\psi_f + \left(L_d - L_q \right) I_d \right] I_q \right\} \tag{17}$$

where λ is the Lagrange constant.

Partial derivatives of (17) can subsequently be zeroed to give:

$$\begin{cases} \dfrac{\partial H}{\partial I_d} = \dfrac{I_d}{\sqrt{I_d^2 + I_q^2}} - \dfrac{3}{2} \lambda n_p \left(L_d - L_q \right) I_q = 0 \\ \dfrac{\partial H}{\partial I_q} = \dfrac{I_q}{\sqrt{I_d^2 + I_q^2}} - \dfrac{3}{2} \lambda n_p \left[\psi_f + \left(L_d - L_q \right) I_d \right] = 0 \\ \dfrac{\partial H}{\partial \lambda} = T_e - \dfrac{3}{2} n_p \left[\psi_f + \left(L_d - L_q \right) I_d \right] I_q = 0 \end{cases} \tag{18}$$

whose solution is:

$$\left(L_d - L_q \right) I_d^2 + \psi_f I_d - \left(L_d - L_q \right) I_q^2 = 0 \tag{19}$$

During flux-weakening and in the second quadrant, (19) can further be rewritten as:

$$I_q = \sqrt{I_d^2 + \frac{\psi_f}{L_d - L_q} I_d}, \quad I_d < 0 \tag{20}$$

which graphically is the dotted hyperbola passing through the origin in Fig. 6. Also shown in the figure are a voltage-limit ellipse that reaches all four quadrants at a low enough speed and a constant-torque curve plotted with (3) for a specific value of T_e. The latter must intersect with the dotted hyperbola at point D, in order for torque T_e to be generated with minimum current and hence optimized efficiency. The flux-weakening voltage along the q-axis must then be fixed at $V_q = V_{FWC1}$ to bring the red linear current trajectory to pass through point D. However, most of the operating range along the negatively sloped current trajectory is in the first quadrant, which may not be preferred.

A simple modification is thus to lower the flux-weakening voltage to $V_q = V_{FWC2}$, while retaining the same desired speed. That causes the linear current trajectory to shift leftward in parallel, so that it passes through point E and the origin. Point E is not far away from point D, while generating the same desired torque T_e. Operating range of the newly shifted current trajectory is also close to the hyperbola of optimal efficiency, and will become even closer at higher speed because of its increasing gradient magnitude according to (11). The proposed tuning of flux-weakening voltage for efficiency optimization is thus effective.

On the other hand, when $\omega_e = \omega_2 > \omega_1$, the voltage-limit ellipse becomes smaller and no longer encircles the origin and efficiency-optimized hyperbola. The operating point that generates the desired torque T_e at the new speed ω_2 will then be the intersection of the smaller voltage-limit ellipse and constant torque curve. The resulting point F has the shortest length from the origin and hence draws the smallest

current, as intended. The flux-weakening voltage must then be changed to $V_q = V_{FWC3}$ at ω_2 to shift the linear current trajectory through point F.

It has therefore been demonstrated that a single current regulator and a mechanism for tuning the flux-weakening voltage V_{FWC} along the q-axis can work with different demanded speeds and torques. They can simultaneously optimize efficiency (or maximize torque and hence load capacity) of the PMSM. Furthermore, with only one current regulator, the proposed scheme is not affected by coupling between current regulators experienced by existing dual-loop scheme. Using only a single current regulator is therefore an attractive alternative.

IV. SLIDING-MODE SPEED CONTROL DURING FLUX-WEAKENING

Referring to the overall block diagram shown in Fig. 1, the next analytical step is to design the outer sliding-mode speed regulator during flux-weakening. Output of this speed regulator is i_d^*, which subsequently has been used as a d-axis current command for the single inner current regulator. Finding i_d^* however requires information about the q-axis voltage V_{FWC} from Section III, speed error $\left(\omega_e^* - \omega_e\right)$ and equivalent load torque $T_L^{'}$. The latter two parameters are described, as follows.

A. SLIDING-MODE SPEED REGULATOR

The proposed sliding-mode speed regulator during flux-weakening can be designed by first defining state variables of the PMSM, as follows:

$$\begin{cases} x_1 = \omega_e^* - \omega_e \\ x_2 = \int_{-\infty}^{t} x_1 \mathrm{d}t = \int_{-\infty}^{t} \left(\omega_e^* - \omega_e\right) \mathrm{d}t \end{cases} \tag{21}$$

where ω_e^* and ω_e are reference and measured electrical angular speeds. Moreover, the usual motor mechanical relationship can be expressed as:

$$T_e - T_L = J\frac{\mathrm{d}\omega_r}{\mathrm{d}t} + B_f\omega_r \tag{22}$$

where T_L is the load torque, J is inertia, B_f is friction coefficient and $\omega_r = \omega_e / n_p$ is the motor mechanical speed.

From (10), (21) and (22), essential state-space equations can then be derived as:

$$\begin{cases} \dot{x_1} = -\dot{\omega}_e = AI_d^2 + BI_d + D \\ \dot{x_2} = x_1 = \omega_e^* - \omega_e \end{cases} \tag{23}$$

where

$$A = \frac{3n_p^2\omega_e}{2J} \cdot \frac{L_d\left(L_d - L_q\right)}{R_s}$$

$$B = \frac{3n_p^2}{2J} \cdot \frac{\psi_f\omega_e L_d - \left(L_d - L_q\right)\left(V_{FWC} - \psi_f\omega_e\right)}{R_s}$$

$$D = -\frac{3n_p^2\psi_f}{2J} \cdot \frac{V_{FWC} - \psi_f\omega_e}{R_s} + \frac{n_p}{J}T_L^{'}$$

$$T_L^{'} = B_f\omega_r + T_L$$

A suitable switching surface is thus:

$$s_1 = x_1 + cx_2 \tag{24}$$

where $c > 0$ is a constant coefficient. Subsequently, by setting $s_1 = 0$, time derivative of (24) becomes:

$$\dot{x_1} = -cx_1 \tag{25}$$

From (21) to (25), speed error x_1 will hence exponentially converge to zero, if its time constant is $1/c$. Coefficient c therefore determines its approaching speed. Further, initial condition of x_2 can be set as:

$$I_0 = \int_{-\infty}^{0} x_1(\tau)\, d\tau = -\frac{x_i}{c} \tag{26}$$

where x_i is the value of x_1 at $t = 0$. That then leads to $s_1|_{t=0} = x_i + c\left(-\frac{x_i}{c}\right) = 0$, or in other words, the sliding motion starts correctly on the switching surface at $t = 0$. This helps to ensure global robustness. After which, time derivative of (24) can be expressed as:

$$\dot{s_1} = \dot{x_1} + cx_1 = AI_d^2 + BI_d + D + cx_1 \tag{27}$$

whose two solutions for I_d are:

$$I_d = \frac{-B \pm \sqrt{B^2 - 4A(D + cx_1 - \dot{s_1})}}{2A} \tag{28}$$

Current I_d can therefore be regulated by speed error x_1. Moreover, during flux-weakening, $A < 0$, implying that only the following solution for I_d will prevail for setting as command i_d^* for the single inner current regulator, as indicated in Fig. 1:

$$I_d = \frac{-B + \sqrt{B^2 - 4A(D + cx_1 - \dot{s_1})}}{2A} \tag{29}$$

For satisfying $I_d < 0$, the following inequality must further be satisfied:

$$\dot{s_1} - cx_1 < D \tag{30}$$

noting too that $D > 0$ tends towards infinity with increasing speed ω_e, if the system is designed according to Section III. Additionally, if the proposed sliding-mode controller is allowed to follow an exponential reaching law to reduce the problem of chattering, the following relationship can be written:

$$\dot{s_1} = -\varepsilon \cdot \Delta \cdot sat\,(s_1) - ks_1 \tag{31}$$

where $\varepsilon > 0$ is the reaching coefficient, $k > 0$ is the exponential reaching coefficient, $\Delta > 0$ is a constant, and:

$$sat\,(s_1) = \begin{cases} 1/\Delta & s_1 > 1/\Delta \\ s_1 & |s_1| < 1/\Delta \\ -1/\Delta & s_1 < -1/\Delta \end{cases}$$

Equation (31) can then always be satisfied by $x_1 > 0$, but not $x_1 < 0$, within which the range of $\dot{s_1}$ becomes limited to $D + cx_1$. Indirectly, they translate to the proposed speed controller performing better with an accelerating command

(increase of ω_e^*), but not a decelerating command (decrease of ω_e^*). The reason is linked to the proposed scheme being designed for operation in the second quadrant of the $i_d - i_q$ plane without considering thoroughly about negative torque. However, in reality, I_d varies within a narrow range due to the limitation of voltage during flux-weakening. Therefore, as long as the sliding-mode function is sensitive enough near the switching surface, the system is soluble.

To verify that, the exponential reaching law in (31) can be referred to, where it has explicitly stated that the sliding speed depends on both ε and k. Additionally, when s_1 is close to zero, the sliding speed is mainly dependent on $-ks_1$, which will ensure that the system stays on the switching surface. The target of robust sliding-mode speed control has therefore been achieved, in addition to either maximum torque or optimal efficiency guaranteed by tuning V_{FWC} properly.

B. EQUIVALENT LOAD-TORQUE OBSERVER

When developing the sliding-mode speed controller, coefficient D in (23) has been derived. Unlike other coefficients in the same equation, coefficient D depends on the equivalent load torque $T_L^{'}$, which is not easy to acquire in practice. Coefficient D is subsequently used in (29) for calculating the d-axis current reference I_d, before feeding it as i_d^* to the single inner current regulator. A mechanism for finding $T_L^{'}$ is thus essential to avoid inaccuracy and large amplitude chattering. Because of that, an equivalent load-torque observer is now developed for integration with the proposed sliding-mode speed controller to enhance its immunity against inaccurate $T_L^{'}$.

State variables of this torque observer can first be defined as:

$$\begin{cases} e_1 = \omega_r - \hat{\omega}_r \\ e_2 = \int_{-\infty}^{t} e_1 \mathrm{d}t = \int_{-\infty}^{t} \left(\omega_r - \hat{\omega}_r\right) \mathrm{d}t \end{cases} \tag{32}$$

where ω_r represents the motor angular speed, and ^represents an estimated value. The actual motor speed ω_r can next be assumed constant in each fast-sampled evaluation period to arrive at the following state-space equations:

$$\begin{cases} \dot{e_1} = -\dot{\hat{\omega}}_r \\ \dot{e_2} = e_1 = \omega_r - \hat{\omega}_r \end{cases} \tag{33}$$

From (33), the switching surface can consequently be designed as:

$$s_2 = e_1 + c_t e_2 \tag{34}$$

where $c_t > 0$ is a constant coefficient. After which, by setting $s_2 = 0$, time derivative of (34) becomes:

$$\dot{e_1} = -c_t e_1 \tag{35}$$

The derived equations from (33) to (35) have thus proven that the speed evaluation error e_1 will converge to zero exponentially, if its time constant is $1/c_t$. Coefficient c_t therefore directly determines its approaching speed. As for e_2, its initial condition can be set as:

$$I_0 = \int_{-\infty}^{0} e_1(\tau)\, d\tau = -\frac{e_i}{c} \tag{36}$$

where e_i is the value of e_1 at $t = 0$. Equation (34) at $t = 0$ then becomes $s_2|_{t=0} = e_i + c\left(-\frac{e_i}{c}\right) = 0$, or in other words, the sliding motion starts correctly on the switching surface at $t = 0$. Global robustness can hence be ensured, and the equivalent load torque can be estimated from:

$$\hat{T_L^{'}} = T_e - J\frac{\mathrm{d}\hat{\omega}_r}{\mathrm{d}t} = T_e - J\frac{\mathrm{d}\omega_r}{\mathrm{d}t} \tag{37}$$

The equivalent load-torque observer is thus relatively straightforward to implement, since it is very similar in structure to the speed regulator. Its estimated $\hat{T_L^{'}}$ can eventually be fed forward to the speed controller for calculating coefficient D.

V. SIMULATED AND EXPERIMENTAL RESULTS

A. SIMULATED RESULTS

Simulations have been performed using the *Piecewise Linear Electrical Circuit Simulation* (PLECS) software. Rated motor parameters simulated are 310V, 2.19A, 550W, $n_p = 8$, $R_s = 3.05\Omega$, $\psi_f = 0.08539$Wb, $L_d = 20.756$mH, $L_q = 24.679$mH, and $J = 0.001\text{kgm}^2$, while inverter parameters simulated are $V_{dc} = 150$V, $V_{smax} = V_{dc}/\sqrt{3} = 86.6$V, and I_{smax}= 2.d75A. With these settings, Fig. 7 shows results obtained with V_{FWC} chosen according to the limited-voltage maximum torque criterion explained in Section III(A). Particularly, to demonstrate the proposed scheme tracking of each steady-state speed, load torque applied to the motor in Fig. 7(b) has been increased gradually by 0.2Nm per second from $T_L = 0$Nm at t= 3s to a maximum of 1.0Nm after t= 8s.

As for the motor speed in Fig. 7(a), it remains at 3000rpm initially, but with conventional flux-weakening control(dual current loop control), it begins to drop gradually at around $t = 8$s due to the maximum electromagnetic torque T_e generated being less than 1.0Nm. On the other hand, with the proposed scheme during flux-weakening, the motor speed remains at 3000rpm with a maximum T_e of 1.0Nm generated. Accompanying this performance is a negative-sloping linear current trajectory shown on the right of Fig. 7(c), which undeniably matches those in Fig. 5. The proposed scheme with limited-voltage maximum-torque criterion has therefore been shown to generate more torque than the conventional method during flux-weakening.

Proceeding on, Fig. 8 shows simulated results for the proposed scheme with efficiency-optimized criterion explained in Section III(B). With a load torque of 0.5Nm and the same speed of 3000rpm, the theoretical operating point must then be at $(I_d, I_q) = (-1.271\text{A}, 0.923\text{A})$, which in Fig. 6, is represented by point F. In Fig. 8(b), this operating point is reached by gradually increasing the load torque by 0.1Nm per second from $T_L = 0$ Nm at $t = 3$s to 0.5Nm after $t = 8$s.

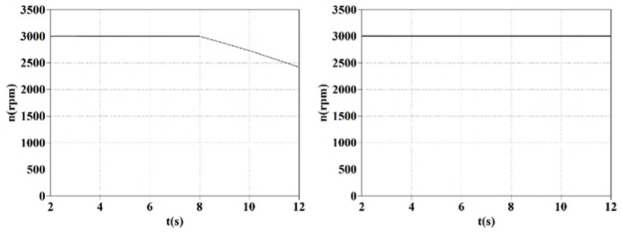

(a) Rotor speed (left: conventional method, right: proposed method)

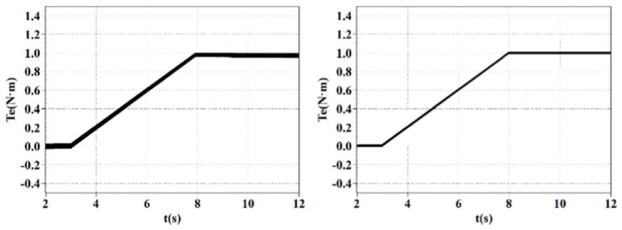

(b) Electromagnetic torque (left: conventional method, right: proposed method)

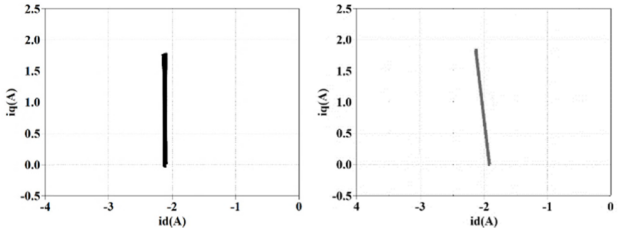

(c) Current trajectory (left: conventional method, right: proposed method)

FIGURE 7. Simulated results for demonstrating limited-voltage maximum-torque criterion.

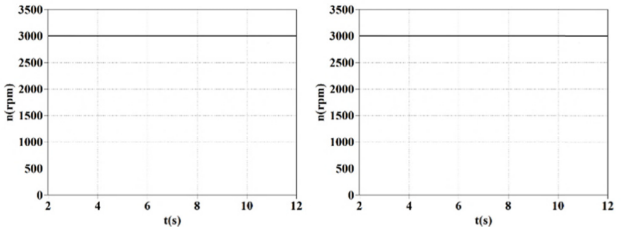

(a) Rotor speed (left: conventional method, right: proposed method)

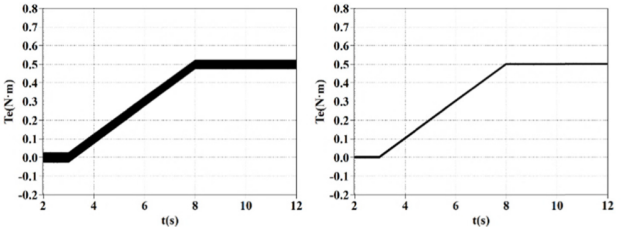

(b) Electromagnetic torque (left: conventional method, right: proposed method)

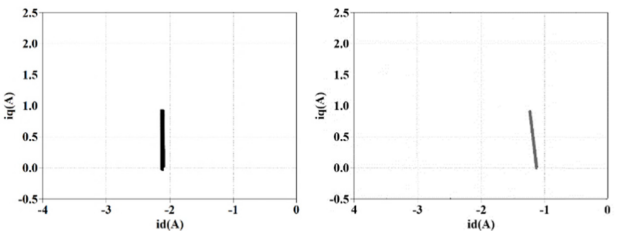

(c) Current trajectory (left: conventional method, right: proposed method)

FIGURE 8. Simulated results for demonstrating optimized-efficiency criterion.

Such increase in load has been met by an equal increase in electromagnetic torque T_e for both schemes. They are therefore able to keep their respective motor speeds constant at 3000rpm, according to Fig. 8(a).

Current trajectories for both schemes in Fig. 8(c) are however different. Their respective terminal points at the final load torque of $T_L = 0.5$ Nm are $(-2.12\text{A}, 0.89\text{A})$ with the conventional scheme and $(-1.27\text{A}, 0.92\text{A})$ with the proposed scheme. Their respective current amplitudes are thus 2.30A and 1.57A, which unambiguously demonstrate that the proposed scheme draws a smaller current, as intended.

The proven single current regulator with two criterions for tuning V_{FWC} is next complemented by the designed outer sliding-mode speed regulator and equivalent load-torque observer. Effectiveness of this regulator-observer combination during flux-weakening can be compared with the conventional outer PI speed regulator when both regulators are sequentially tested with a load disturbance, a dc-bus disturbance and a stator-resistance perturbation. Fig. 9 shows the results at 3000rpm with the load increased from zero to $T_L = 0.4$ Nm at $t = 3$s. This causes the PI-regulated speed to drop rapidly to 2800rpm as in Fig. 9(a), before it recovers slowly to 3000rpm after $t = 3.3$s.

Such drop does not occur with the proposed speed regulator, which only chatters slightly for 0.1s. This improvement is possible, because of the fast sliding-mode action, which in Fig. 9(b), corresponds to the large instantaneous electromagnetic torque of $T_e = 0.75$ Nm generated for countering the load torque. With the PI speed regulator, T_e is only 0.42Nm. The proposed sliding-mode speed regulator is thus less immune to load disturbances. As for dc-bus disturbances, the motor has been tested with a drop of dc-bus voltage from 150V to 120V at $t = 3$s, as shown in Fig. 10(a). During this period, the load is 0.8Nm at 3000rpm. Fig. 10(b) shows that with the PI speed regulator, the motor speed begins to fall from $t = 3$s until it reaches 2400rpm at $t = 4$s. The drop in dc-bus voltage has however not affected the proposed sliding-mode speed regulator, hence demonstrating its immunity towards dc-bus disturbances.

Lastly, the two speed regulators have been tested at no load, but with the motor stator resistance gradually increased from $R_s = 3.05\Omega$ before $t = 3$s to 9.15Ω after $t = 7$s, as seen from Fig. 11(a). During this time, Fig. 11(b) shows the PI-regulated speed dropping from 3000rpm before $t = 6$s to 2800rpm after $t = 7$s. But, with the sliding-mode speed regulator, no change in speed has been observed, because of its immunity towards stator-resistance perturbations. Collectively, the results have

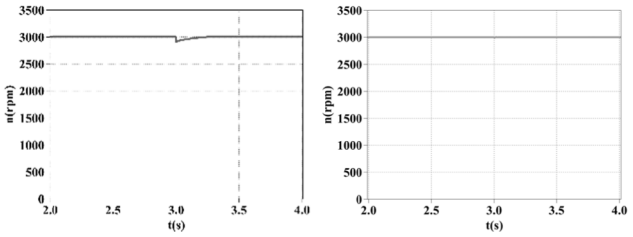

(a) Rotor speed (left: PI, right: sliding-mode)

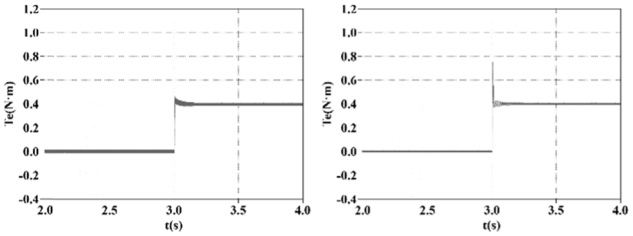

(b) Electromagnetic torque (left: PI, right: sliding-mode)

FIGURE 9. Simulated results for demonstrating load-disturbance immunity.

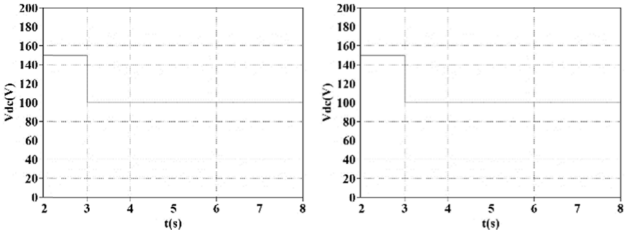

(a) DC-bus voltage (left: PI, right: sliding-mode)

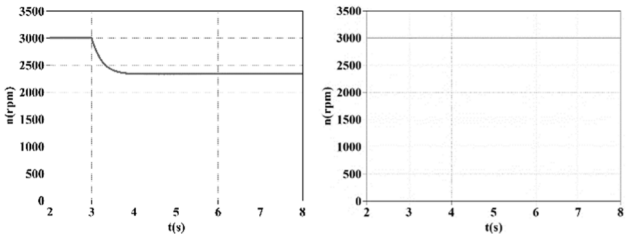

(b) Rotor speed (left: PI, right: sliding-mode)

FIGURE 10. Simulated results for demonstrating dc-bus-disturbance immunity.

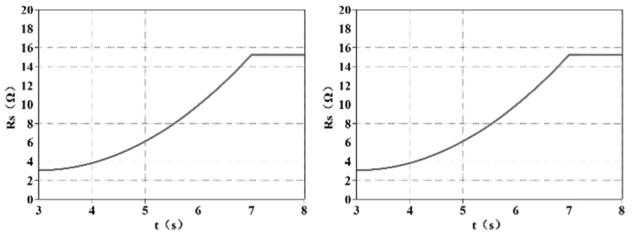

(a) Stator resistance (left: PI, right: sliding-mode)

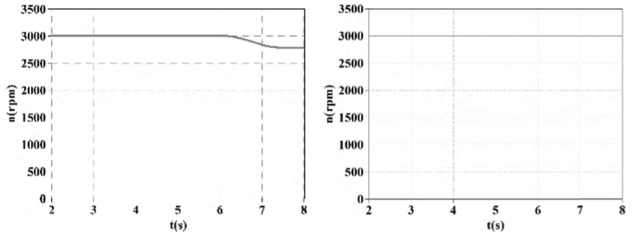

(b) Rotor speed (left: PI, right: sliding-mode)

FIGURE 11. Simulated results for demonstrating stator-resistance-perturbation immunity.

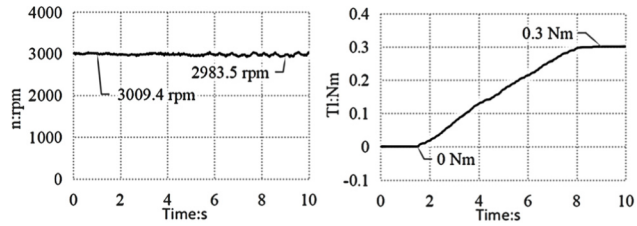

(a) Rotor speed (b) Electromagnetic torque

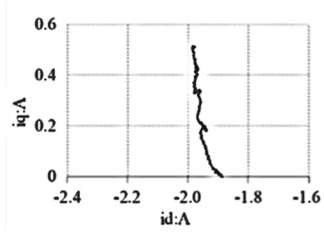

(c) Current trajectory

FIGURE 12. Experimental results for demonstrating limited-voltage maximum-torque criterion.

therefore verified the proposed scheme in Fig. 1, consisting of the sliding-mode speed regulator, equivalent load-torque observer and a single inner current regulator with two criterions for tuning the flux-weakening voltage.

B. EXPERIMENTAL RESULTS

In addition to simulations, the proposed scheme has been tested in experiments. Fig. 12 shows results with V_{FWC} tuned according to the limited-voltage maximum torque criterion found in Section III(A). The load condition tested in Fig. 12(b) is from no load to $T_L = 0.3$Nm, subjected to conditional constraints of the experimental platform. Regardless of that, the motor speed in Fig. 12(a) remains nearly constant with values of 3009.4rpm and 2983.5rpm read before and after the load change. During the change, Fig. 12(c) has also confirmed that the current trajectory is linear and negative-sloping, and hence in consistent with theory. Fig. 13 then shows results with the efficiency-optimized criterion and the same load increase from zero to 0.3Nm. The load increase has been shown in Fig. 13(a), while Fig. 13(b) confirms that the motor speed remains almost constant at around 3010.5rpm and 3012.3rpm, before and after the load change. This is again achieved with a negative-sloping linear current trajectory, as shown in Fig. 13(c).

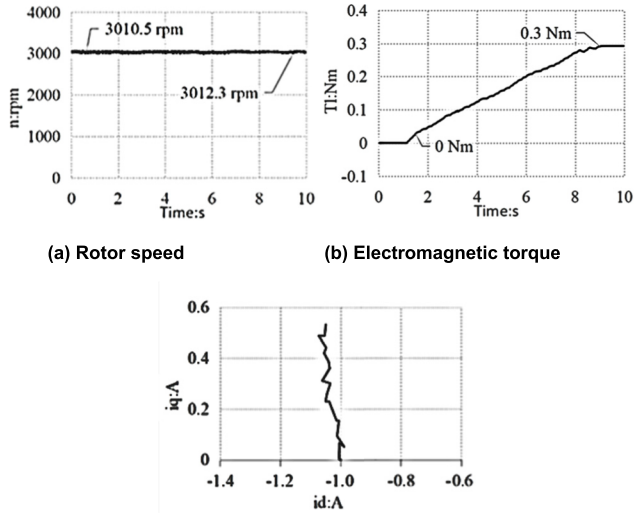

(a) Rotor speed (b) Electromagnetic torque

(c) Current trajectory

FIGURE 13. Experimental results for demonstrating optimized-efficiency criterion.

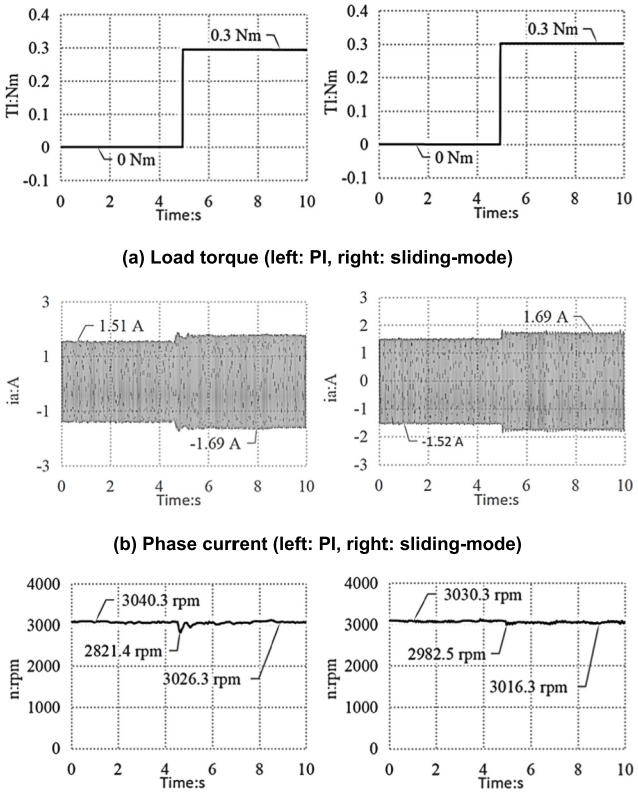

(a) Load torque (left: PI, right: sliding-mode)

(b) Phase current (left: PI, right: sliding-mode)

(c) Rotor speed (left: PI, right: sliding-mode)

FIGURE 14. Experimental results for demonstrating load-disturbance immunity.

Proceeding to the sliding-mode speed regulator with the equivalent load-torque observer, Fig. 14(a) shows the experimental load suddenly raised from zero to $T_L = 0.3$Nm at $t = 5$s. Both conventional PI speed regulator and proposed regulator-observer combination have been tested with Fig. 14(b) showing their corresponding peak currents

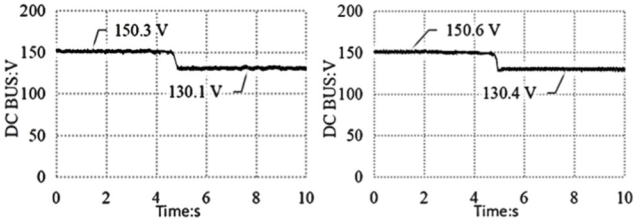

(a) DC-bus voltage (left: PI, right: sliding-mode)

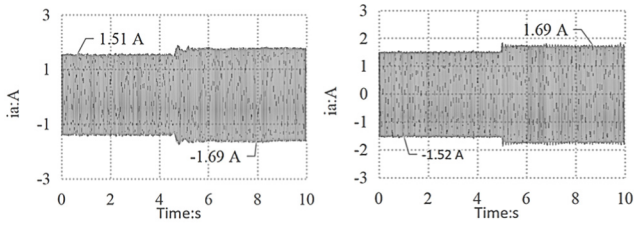

(b) Phase current (left: PI, right: sliding-mode)

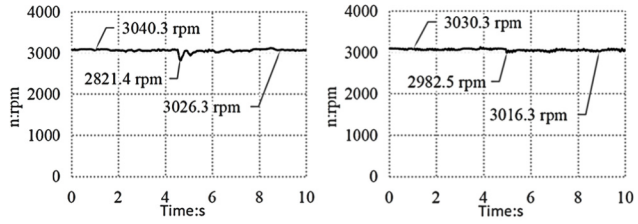

(c) Rotor speed (left: PI, right: sliding-mode)

FIGURE 15. Experimental results for demonstrating dc-bus-disturbance immunity.

supplied to the motor being almost the same throughout the transition. However, current waveforms with the PI speed regulator are more oscillatory. This causes the PI-regulated speed to be more oscillatory in Fig. 14(c) with its value dropping rapidly from 3040.3rpm to 2821.4rpm, before rising back to 3026.3rpm after a few oscillatory cycles. Current and speed waveforms of the proposed sliding-mode regulator are however less oscillatory with its speed dropping lesser from 3030.3rpm to 2982.5rpm, before returning to 3016.3rpm after a shorter recovery time.

Immunities of the regulators have next been tested with a load of $T_L = 0.1$ Nm, but with the dc-bus voltage suddenly reduced from about 150V to 130V, as in Fig. 15(a). This causes the peak current supplied to the motor to rise gradually from 1.23A to 1.51A with the PI speed regulator, but almost immediately from 1.25A to 1.49A with the proposed sliding-mode speed regulator, as viewed from Fig. 15(b). Correspondingly, the PI-regulated speed in Fig. 15(c) falls from 3000.5rpm to 2834.0rpm, before returning to 3009.2rpm in about 4s. On the other hand, the sliding-mode-regulated speed falls from 3004.1rpm to 2949.5rpm, before returning to 3000.985rpm in about 1s. The proposed sliding-mode regulator is therefore dynamically faster and more immune to dc-bus disturbances.

As for parameter perturbations, including those of the stator resistance R_s, they cannot be experimentally controlled

and hence not explicitly performed. Nonetheless, uncontrolled parameter perturbations always exist in practice, including during the capturing of Fig. 14 and Fig. 15. Results in these two figures have therefore indirectly proven accurate performance of the proposed sliding-mode regulator, even when subjected to realistic experimental conditions.

VI. CONCLUSION

This paper presents a flux-weakening scheme, which uses only a single inner current regulator and a mechanism for tuning the flux-weakening voltage. Criterion targeted during the tuning can either be to achieve maximum electromagnetic torque generated or optimal efficiency with minimum current drawn by the motor. These inner control entities are then complemented by an outer sliding-mode speed regulator and an equivalent load-torque observer designed to filter away disturbances dynamically fast. Simulated and experimental results have verified such immunity and robustness, in addition to either an increase in load-torque capacity or an improved light-load efficiency during flux weakening.

REFERENCES

[1] S. Morimoto, M. Sanada, and Y. Takeda, "Wide-speed operation of interior permanent magnet synchronous motors with high-performance current regulator," *IEEE Trans. Ind. Appl.*, vol. 30, no. 4, pp. 920–926, Jul. 1994.
[2] C.-T. Pan and S. M. Sue, "A linear maximum torque per ampere control for IPMSM drives over full-speed range," *IEEE Trans. Energy Convers.*, vol. 20, no. 2, pp. 359–366, Jun. 2005.
[3] B.-H. Bae, N. Patel, S. Schulz, and S.-K. Sul, "New field weakening technique for high saliency interior permanent magnet motor," in *Proc. 38th IAS Annu. Meeting Conf. Rec. Ind. Appl. Conf.*, Salt Lake City, UT, USA, vol.2, Oct. 2003, pp. 898–905.
[4] R. U. Lenke, R. W. De Doncker, M.-S. Kwak, T.-S. Kwon, and S.-K. Sul, "Field weakening control of interior permanent magnet machine using improved current interpolation technique," in *Proc. 37th IEEE Power Electron. Spec. Conf.*, Jeju-do, South Korea, Jun. 2006, pp. 1–5.
[5] J. Ottosson and M. Alakula, "A compact field weakening controller implementation," in *Proc. Int. Symp. Power Electron., Electr. Drives, Autom. Motion*, Taormina, Italy, May 2006, pp. 696–700.
[6] Y.-D. Yoon, W.-J. Lee, and S.-K. Sul, "New flux weakening control for high saliency interior permanent magnet synchronous machine without any tables," in *Proc. Eur. Conf. Power Electron. Appl.*, Aalborg, Denmark, Sep. 2007, pp. 1–7.
[7] S. D. Sudhoff, K. A. Corzine, and H. J. Hegner, "A flux-weakening strategy for current-regulated surface-mounted permanent-magnet machine drives," *IEEE Trans. Energy Convers.*, vol. 10, no. 3, pp. 431–437, Sep. 1995.
[8] P.-Y. Lin and Y.-S. Lai, "Novel voltage trajectory control for flux weakening operation of surface mounted PMSM drives," in *Proc. IEEE Ind. Appl. Soc. Annu. Meeting*, Edmonton, AB, Canada, Oct. 2008, pp. 1–8.
[9] J.-M. Kim and S.-K. Sul, "Speed control of interior permanent magnet synchronous motor drive for the flux weakening operation," *IEEE Trans. Ind. Appl.*, vol. 33, no. 1, pp. 43–48, Jan./Feb. 1997.
[10] M. C. Paicu, L. Tutelea, G.-D. Andreescu, F. Blaabjerg, C. Lascu, and I. Boldea, "Wide speed range sensorless control of PM-RSM via 'active flux model,'" in *Proc. IEEE Energy Convers. Congr. Expo.*, San Jose, CA, USA, Sep. 2009, pp. 3822–3829.
[11] S. Chi, L. Xu, and Z. Zhang, "Efficiency-optimized flux-weakening control of PMSM incorporating speed regulation," in *Proc. IEEE Power Electron. Spec. Conf.*, Orlando, FL, USA, Jun. 2007, pp. 1627–1633.
[12] L. Xu, Y. Zhang, and M. K. Guven, "A new method to optimize q-axis voltage for deep flux weakening control of IPM machines based on single current regulator," in *Proc. Int. Conf. Electr. Mach. Syst.*, Wuhan, China, Oct. 2008, pp. 2750–2754.
[13] Y. Zhang, L. Xu, M. K. Guven, S. Chi, and M. S. Illindala, "Experimental verification of deep field weakening operation of a 50-kW IPM machine by using single current regulator," in *Proc. IEEE Energy Convers. Congr. Expo.*, San Jose, CA, USA, Sep. 2009, pp. 3647–3652.
[14] H. Yang, S. Chi, and G. Song , "A novel algorithm for improving load and immunity of permanent magnet synchronous motor based on single current regulator," *Electr. Mach. Control Appl.*, vol. 45, no. 5, pp. 77–82 and 87, May 2018.

XUE LI received the B.S. and M.S. degrees in control science and engineering from the Hebei University of Technology, Tianjin, China, in 2010, where she is currently pursuing the Ph.D. degree in electrical engineering. Her current research interests include motor vector control and sliding mode variable structure control in the field of power electronics.

CONG LIU received the B.S. degree in control science and engineering from the Hebei University of Technology, Tianjin, China, in 2017, where she is currently pursuing the M.S. degree in electrical engineering. Her current research interests include sliding mode variable structure control in the field of power electronics.

SHANG WU received the B.S. degree in electrical engineering from the Hebei University of Technology, Tianjin, China, in 2018, where he is currently pursuing the M.S. degree in electrical engineering. His current research interests include motor vector control.

SONG CHI (S'04–M'07) received the B.S. degree in electrical engineering from Northeastern University, Shenyang, China, in 1993, the M.S. degree in electrical engineering from Tsinghua University, Beijing, China, in 2000, and the Ph.D. degree in electrical engineering from The Ohio State University, Columbus, in 2007.

He was a Senior Engineer with the Research and Engineering Center, Whirlpool Corporation, and also a Senior Engineer with the Global Research Center, General Electric, Niskayuna, NY, USA. He is currently a Distinguished Professor with the School of Electrical Engineering, Hebei University of Technology. His research interests include high frequency power electronics and motor vector control.

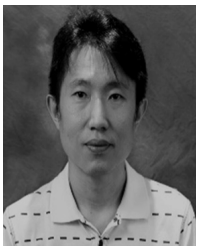

POH CHIANG LOH received the B.Eng. (Hons.) and M.Eng. degrees from the National University of Singapore, in 1998 and 2000, respectively, and the Ph.D. degree from Monash University, Australia, in 2002, all in electrical engineering. He is currently with The Chinese University of Hong Kong, Hong Kong. His current research interest includes power converters and their grid applications.